ADVANCED MATERIALS
www.advmat.de

Facilitated Water Transport through Graphene Oxide Membranes Functionalized with Aquaporin-Mimicking Peptides

Chang Seon Lee, Moon-ki Choi, Ye Young Hwang, Hyunki Kim, Moon Ki Kim, and Yun Jung Lee**

Water purification by membranes is widely investigated to address concerns related to the scarcity of clean water. Achieving high flux and rejection simultaneously is a difficult challenge using such membranes because these properties are mutually exclusive in common artificial membranes. Nature has developed a method for this task involving water-channel membrane proteins known as aquaporins. Here, the design and fabrication of graphene oxide (GO)-based membranes with a surface-tethered peptide motif designed to mimic the water-selective filter of natural aquaporins is reported. The short RF8 (RFRFRFRF, where R and F represent arginine and phenylalanine, respectively) octapeptide is a concentrated form of the core component of the Ar/R (aromatic/arginine) water-selective filter in aquaporin. The resulting GO-RF8 shows superior flux and high rejection similar to natural aquaporins. Molecular dynamics simulation reveal the unique configuration of RF8 peptides and the transport of water in GO-RF8 membranes, supporting that RF8 effectively emulates the core function of aquaporins.

Clean and fresh water is essential for all humans. However, clean water scarcity has become a major problem,[1] with water contamination causing clean water shortages. Nearly all human activities cause water contamination. Water is polluted by heavy metal ions, organic dyes, and micropollutants, which have received increasing attention.[2] As a result, there is growing interest in the development of methods to purify water.

Treating contaminated water with membranes is an important technology and is considered a green technology with many advantages, such as low chemical usage and low energy consumption, compared to other water treatment methods.[3,4] Current water treatment membranes show significantly high rejection for salts[5–8] but low permeability.[9] However, the use of artificial membranes is limited because of their cost, flux, and fouling.[10] Separation processes for current artificial membrane are mostly based on size sieving or the solution–diffusion mechanism.[11] Numerous studies have been conducted to develop other separation mechanisms, such as replicating the features of biological membranes that use specific processes to separate water and other ions or molecules.[12–14]

Among the many biological channels in nature, those for water known as aquaporins (AQPs) were recently shown to have properties that may be useful for water treatment. AQPs have high water permeability and effectively reject other ionic species and molecules.[15–18] Various studies have attempted to reproduce these novel features of AQPs outside of cell membranes. The basic approach for mimicking AQPs is to extract proteins from AQPs and reconstitute them in vesicles or a synthetic bilayer because many biological channels lose their characteristics outside of their biological environment. The incorporation of extracted AQPs embedded in either biological or synthetic bilayers is a highly reliable method for retaining the performance of natural AQPs;[12–14] however, it is difficult to control structural defects and conduct scale-up because of the fragile mechanical characteristics of these proteins. Rather than transferring the whole AQP structure, the key function of these proteins can be artificially materialized by mimicking only the core components for the function. Here, we simplified the core components and designed functional molecules that can reproduce the core function of AQPs. The designed functional molecules were then incorporated into a solid-state scaffold to develop artificial water-selective channels with improved mechanical strength.

Although the structure and basic function of AQPs have been examined previously,[19,20] they are not completely understood. The AQP protein typically forms an hourglass-shaped morphology with two main constriction sites that act as selective filters for water. The aromatic/arginine (Ar/R) selectivity filter is located at the narrowest part of the pore and thus is regarded as the most important factor in selective transport. The amino acids in the Ar/R filter vary in the different AQP families, with arginine (Arg, R) and phenylalanine (Phe, F) as the most highly

C. S. Lee, Y. Y. Hwang, Prof. Y. J. Lee
Department of Energy Engineering
Hanyang University
Seoul 04763, Republic of Korea
E-mail: yjlee94@hanyang.ac.kr
M.-K. Choi, H. Kim, Prof. M. K. Kim
School of Mechanical Engineering
Sungkyunkwan University
Suwon 16419, Republic of Korea
E-mail: mkkim@me.skku.ac.kr
The ORCID identification number(s) for the author(s) of this article can be found under https://doi.org/10.1002/adma.201705944.

DOI: 10.1002/adma.201705944

conserved amino acids in human aquaporin AQP-1. The hydrophobic aromatic group of phenylalanine weakens water–water hydrogen bonds to orient water molecules for rapid water transport.[20] The positively charged arginine rejects positive ions and protons.[21] In addition, molecules larger than the Ar/R constriction site are rejected by desolvation effects[19] and size sieving.[21] Using these selection mechanisms, Ar/R constriction sites rapidly transport water molecules and effectively reject other salts. We designed a functional molecule composed of R and F as the simplified core component for water selection, which is expected to play a similar role as the natural Ar/R selectivity filter.

Using an appropriate solid-state membrane is another important task in constructing artificial water selective channels. Among the many available solid-state scaffolds, graphene oxide (GO) has several advantages as a water treatment membrane.[22] GO is oxidized graphene composed of flat layers of a graphene framework with various oxygen-containing groups such as carbonyl (C=O), carboxyl (−COOH), and hydroxyl (−OH).[23] Because these oxygen-containing groups are on the surface of GO, GO can be modified with desired functional molecules.[24,25] Moreover, the interlayer space between stacked GO flakes can be used for molecular transport, such as in laminated GO membranes.[26] Pristine GO membranes show relatively high pure water flux and moderate rejection of salts.[27] Because of the versatility in anchoring functional molecules on its surface, GO can be used to develop artificial water-selective channels. Here, we used GO films as solid-state water treatment membranes supported on polycarbonate (PC) or mixed cellulose ester (MCE) layers for mechanical reinforcement because the thin GO films generally do not have sufficient mechanical strength to support the pressure-driven water transport in this study. GO was functionalized with a synthetic peptide motif simulating the Ar/R aquaporin filter. The octapeptide sequence RFRFRFRF (Arg-Phe-Arg-Phe-Arg-Phe-Arg-Phe), named RF8, was immobilized on the GO surface to produce GO-RF8. The GO-RF8 ultrafiltration membrane achieved ultrafast water permeation without compromising the rejection of unwanted substances. The unique behavior of RF8 peptides was verified by molecular dynamics simulation, revealing the unique configuration of RF8 peptides and facilitated water transport in GO-RF8 membranes. Rather than transferring whole AQPs from natural cells, we successfully reproduced the core function of AQPs using this simple short peptide RF8 as the concentrated form of the water-selective filter in AQPs.

The process of GO-RF8 membrane fabrication is schematically presented in Figure S1 (Supporting Information). The AQP-mimicking peptide motif, RF8, was functionalized on the carboxylic groups of the GO surface. Pristine GO was treated with chloroacetic acid under strongly basic conditions and neutralized with HCl. This process converts surface oxygen-containing groups such as hydroxyl, ester, and epoxide to carboxylic groups. The increased number of carboxylic groups on the GO surface enhances the efficiency of the peptide grafting onto the GO surface. Carboxylated GO with an increased number of COOH groups was named GO-COOH. RF8 was then anchored to the GO-COOH surface by a carbodiimide coupling (EDC/NHS) method.[28]

The resulting GO-RF8 was not well dispersed in water under neutral conditions. The degree of dispersion in the GO-based colloid was closely related to defects in the vacuum-filtered membrane. Therefore, it is important to form a well-dispersed GO-based colloid to produce a membrane with few defects. Pristine or carboxylated GO form well-dispersed aqueous colloids because of their highly negative surface charges.[29] Therefore, the poor dispersion of GO-RF8 may be related to surface charge modification by positively charged arginine (R) residues in RF8, which reduced the electrostatic repulsion between the GO sheets. It is known that absolute zeta potential values higher than 30 mV ensure the stability of the dispersion with sufficient electrostatic repulsion.[30] Because the zeta potential and colloidal stability of an electrostatically stabilized dispersion strongly depend on pH, the zeta potentials of GO-RF8 solution under neutral (pH 7), acidic (pH 4.5), and alkaline (pH 9) conditions were measured. As shown in Figure S2 (Supporting Information), the zeta potentials of GO-RF8 at pH 7.5 and 4.5 were positive, but the absolute values were below 30 mV. At pH 9, the zeta potential became negative with an absolute value higher than 30 mV. We concluded that GO-RF8 formed a stable aqueous colloid under alkaline conditions; therefore, GO-RF8 colloids were prepared at pH 9. The GO-RF8 solution was vacuum-filtered through a track-etched PC or MCE membrane with a pore size of 0.2 μm as a support.

Successful functionalization of RF8 peptide on the GO surface was confirmed by X-ray photoelectron spectroscopy (XPS). Pristine GO has many oxygenated surface functional groups, such as hydroxyl (−OH), epoxide (−O−), and carboxyl (−COOH) groups. The high-resolution C 1s spectra of GO in Figure S3A (Supporting Information) show that hydroxyl and epoxide groups were the dominant functional groups of GO among the many oxygenated surface functional groups. After functionalizing RF8 peptides on GO, the peak intensities of the hydroxyl and epoxide groups clearly decreased, while those of carbonyl (C=O) and carboxylic groups increased (Figure S3B, Supporting Information). Amide bonds and carboxylic groups in the RF8 peptides contribute to the increased intensity of carbonyl and carboxylic peaks in the C1s of GO-RF8. The presence of nitrogen in GO-RF8, which is absent in GO, was verified, as shown in Figure S3C (Supporting Information). The XPS signals of nitrogen in GO-RF8, originating from the amide bonds and arginine side groups of RF8 peptides, also confirmed the successful functionalization of RF8 peptides on the GO surface.

The permeate flux of pure water and the rejection rate of methyl blue dye molecules through the GO-RF8 membranes were evaluated in a pressure-driven dead-end filtration cell (a stirred cell, as described in the following text). For comparison, GO was functionalized with two other octapeptides, Copep and random, to generate GO-Copep and GO-random. Copep is a cobalt ion-binding peptide with a sequence of EPGHDAVP (Glu-Pro-Gly-His-Asp-Ala-Val-Pro).[28] The random peptide with a sequence of GLDGSAVD (Gly-Leu-Asp-Gly-Ser-Ala-Val-Asp) was previously selected randomly from a library.[31] Carboxylated GO, GO-COOH, was tested as a negative control.

The permeate flux of pure water through the GO-based membranes (GO-COOH, GO-RF8, GO-Copep, and GO-random) with the same mass loading (0.1 mg cm^{-2}) at an applied pressure of 5 bar is shown in **Figure 1**A. The GO-RF8 membrane showed the highest permeate flux (680 L m^{-2} h^{-1} (LMH)), while the GO-COOH membrane showed the lowest permeate

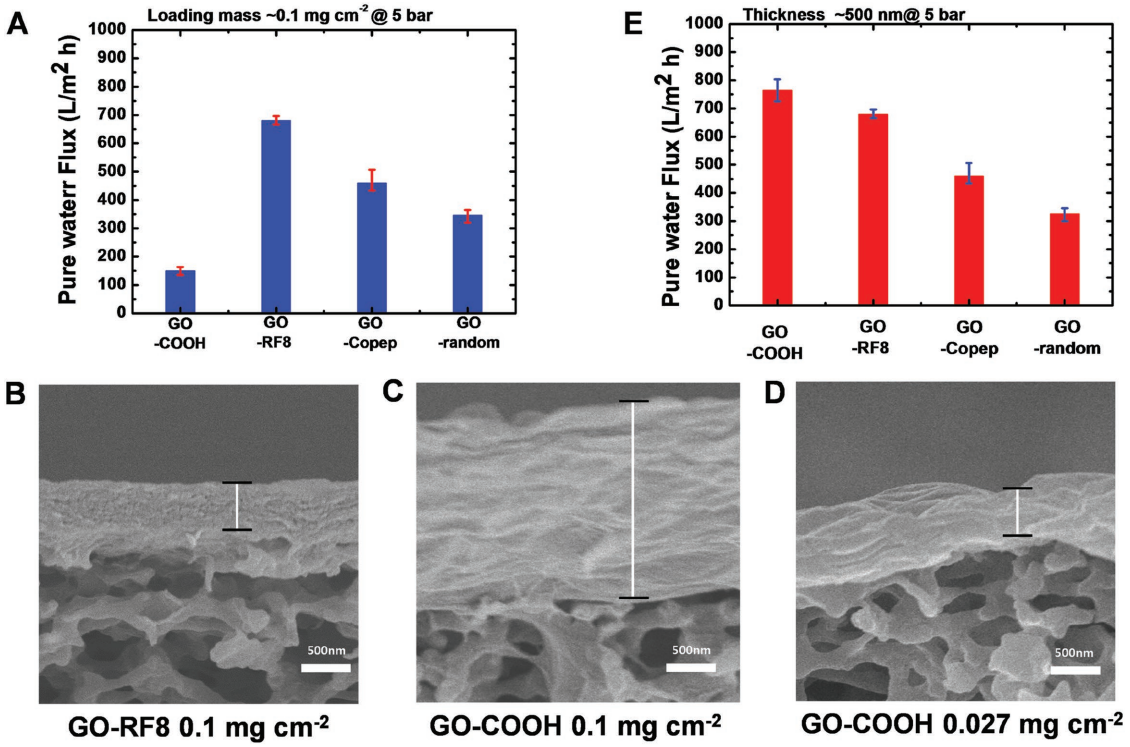

Figure 1. Graphene-oxide-based membranes functionalized with peptides. A) Permeated pure water flux of GO-COOH, GO-RF8, GO-Copep, and GO-random membranes at 5 bar at the same mass loading (0.1 mg cm^{-2}). Cross-sectional SEM image of B) GO-RF8 loading with mass loading of 0.1 mg cm^{-2}, C) GO-COOH loading with mass loading 0.1 mg cm^{-2}, and D) GO-COOH loading with mass loading 0.027 mg cm^{-2}. E) Permeated pure water flux through GO-COOH, GO-RF8, GO-Copep, and GO-random membranes at the same thickness of 500 nm.

flux (150.95 LMH). The permeate flux of GO-Copep and GO-random membranes was lower than that of the GO-RF8 membrane. When the thickness of the GO-based membranes at the same mass loading of 0.1 mg cm^{-2} was examined, however, GO-RF8 had a thickness of ≈500 nm (Figure 1B), which is only 25% of that of GO-COOH (≈2 µm) (Figure 1C). This was likely because GO-RF8 has a higher mass/volume ratio than GO-COOH because RF8 peptides of high molecular weight (1231.45 g mol^{-1}) were anchored on GO-RF8. The lower flux of GO-COOH at the same mass loading is thus due to the higher thickness of the GO-COOH membrane. To exclude the possibility that the highest flux of GO-RF8 was related with its thickness, we set the thickness of the GO-based membrane to ≈500 nm. When the deposited mass of GO-COOH was 0.027 mg cm^{-2}, the thickness was ≈500 nm (Figure 1D). The thickness of GO-Copep and GO-random was also adjusted to ≈500 nm. The permeate flux of pure water through the GO-based membrane at the same thickness was evaluated and is compared in Figure 1E. At the same membrane thickness, GO-COOH showed the highest flux of pure water (765 LMH). Among the octapeptide-functionalized membranes, GO-RF8 still showed the highest pure water permeate flux.

The pressure response of the 500 nm thick GO-RF8 membranes is presented in **Figure 2**A. The graph shows the permeate flux and rejection rate of the aqueous methyl blue (MB) dye solution from 1.5 to 5 bar. The total permeate flux

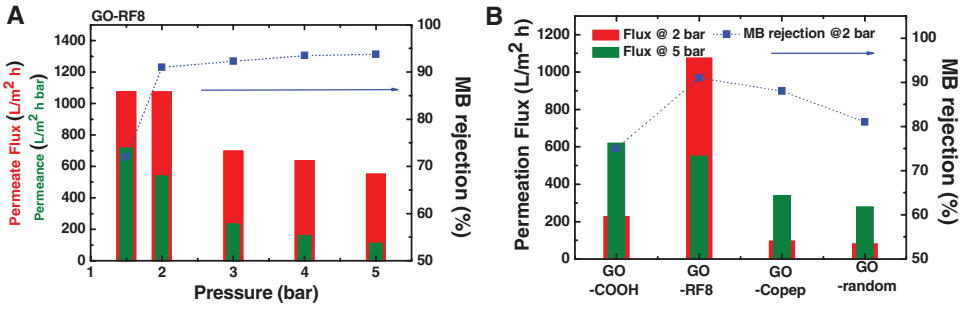

Figure 2. Permeation test of methyl blue aqueous solutions through GO-RF8 membranes. A) Pressure dependence of the permeate flux and rejection rate of MB through GO-RF8 membrane. B) Permeate flux through GO-COOH, GO-RF8, GO-Copep, and GO-random membranes at 2 and 5 bar. Rejection rate of MB (right axes) is for the corresponding membranes at 2 bar. All GO-based membranes tested have the same thickness of 500 nm.

A

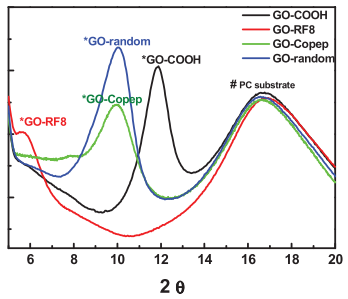

B

	Peptide sequence	Peptide molecular weight (g mole^{-1})	*Channel size (Å)
GO-RF8	RFRFRFRF	1231.46	16.24
GO-Copep	EPGHDAVP	820.86	9.89
GO-Random	GLDGSAVD	732.74	9.80
GO-COOH	Control (pristine)	-	8.70

Figure 3. Estimation of the channel size of GO-based membranes at the same thickness of 500 nm. A) X-ray diffraction of GO-COOH, GO-RF8, GO-Copep, and GO-random membranes. B) Table showing peptide sequence, peptide molecular weight, and estimated channel size.

(L m^{-2} h^{-1} (LMH)) is illustrated as red bars, and the pressure normalized permeate flux (L m^{-2} h^{-1} bar^{-1} (LMHbar)) is illustrated as green bars. The total pure water flux through the GO-RF8 membranes increased from 550 to 1074 LMH when the driving pressure decreased from 5 to 1.5 bar (Figure 2A, red bars). The pressure-normalized flux also increased with decreasing pressure (Figure 2A, green bars). The rejection rate of the MB molecules increased with pressure from 72% at 1.5 bar to 94% at 5 bar. The pressure response of GO-RF8 is unusual because the permeate flux of a typical membrane is directly proportional to the driving pressure. In most polymer membranes, pressure-normalized flux is invariant or slightly reduced because of the compression or densification of the porous structures. The resulting total flux nearly linearly increases with pressure. Because of compression or densification, the rejection rate of small molecules typically increases slightly with pressure.[32] GO-RF8 showed an increasing rejection rate with pressure, which is seen in common polymer membranes, indicating that the channels were compressed under high pressure. The decreased total flux of GO-RF8 at high pressure indicates that the compression of the channels in GO-RF8 under pressure was much more severe than in common membranes because of the remarkable reduction in the channel size. In contrast, the channel size decrease in common membranes under pressure does not induce a reduction in the total flux at higher pressure.

To determine the origin of the unusual pressure dependence of GO-RF8, the pressure response of other GO-based membranes (thickness of 500 nm) was examined. Because GO-RF8 showed optimum flux-rejection performance at 2 bar, we selected 2 bar as a reference condition and compared the flux of GO-based membranes at 2 and 5 bar. Unlike GO-RF8, other GO-based membranes showed a permeate flux proportional to the applied pressure in Figure 2B. The permeate flux through the GO-COOH membrane decreased from 765 to 227 LMH as the pressure decreased from 5 to 2 bar. GO-Copep and GO-random membranes also showed decreased permeation with decreasing pressure. Thus, the severe channel size decrease in GO-RF8 at high pressure may not be related to the softness of the GO platform itself because other GO-based membranes behaved similarly to the common polymeric membranes.

To compare the channel structure of GO-RF8 with those of other GO-based membranes, the interplanar distance of each membrane was investigated by X-ray diffraction (XRD). The ≈500 nm thick GO-based membranes on the PC support were the same membranes examined in the permeation test. The XRD spectrum of each GO-based membrane is presented in **Figure 3**A. The diffraction peaks of each membrane were positioned at $2\theta = 11.5°$ for GO-COOH, 10.05° for GO-random, 9.95° for GO-Copep, and 5.8° for GO-RF8. The interplanar distance was estimated with Bragg's law ($n\lambda = 2d \sin \theta$). The corresponding interplanar separation was 7.70 Å for GO-COOH, 8.80 Å GO-random, 8.89 Å for GO-Copep, and 15.24 Å for GO-RF8. The channel size of the GO-based membrane is a free space between stacked layers. Considering that GO-based membranes swell with an additional water absorption layer that is ≈5 Å thick, and the thickness of the GO sheet is ≈4 Å,[33] the channel size of the GO-based membranes was 8.70 Å for GO-COOH, 9.89 Å for GO-Copep, 9.80 Å for GO-random, and 16.24 Å for GO-RF8 membrane. The channel size increased with increasing molecular weight of the peptides grafted on GO (Figure 3B).

The peptide size is generally proportional to molecular weight, although the linear length depends on the conformation. In addition, large molecules anchored to the GO surface can widen the galleries because the GO membranes are 2D laminates and are free to expand in the vertical direction when stacked. Thus, structural characteristics of anchored peptides on the GO surface may cause changes in the channel size, flux, and MB rejection. To support this hypothesis, the conformational changes of octapeptides used in this study were examined by molecular dynamics (MD) simulations. As shown in **Figure 4**, the conformational changes of RF8, Copep, and random peptides in water under ambient conditions (300 K and 1 atm) were simulated. Although the molecules showed a similar backbone length (≈2.8 nm) when fully extended, RF-8 had larger side chains compared to Copep and random peptides, as reflected in its higher molecular weight inducing a larger solvent-accessible surface area (SASA, 1588 Å^2). Thus, GO-RF8 may have a larger channel size due to this strong side chain effect (Figure 4A). In contrast, Copep (SASA: 1134 Å^2) and random (SASA: 1015 Å^2) peptides have smaller side chains and can easily generate a variety of backbone conformations (e.g., sharp folding) (Figure 4B,C). When we consider time-averaged motions of the peptides, the size difference among the peptides becomes larger since Copep and random peptides fold and unfold more frequently than RF8. Movies S1–S3 of the conformational transition of each peptide are provided as the Supporting Information. Both the average and minimum end-to-end distances of RF8 (19.87 and 12.39 Å) are also larger than those of Copep (17.12 and 7.15 Å) and random

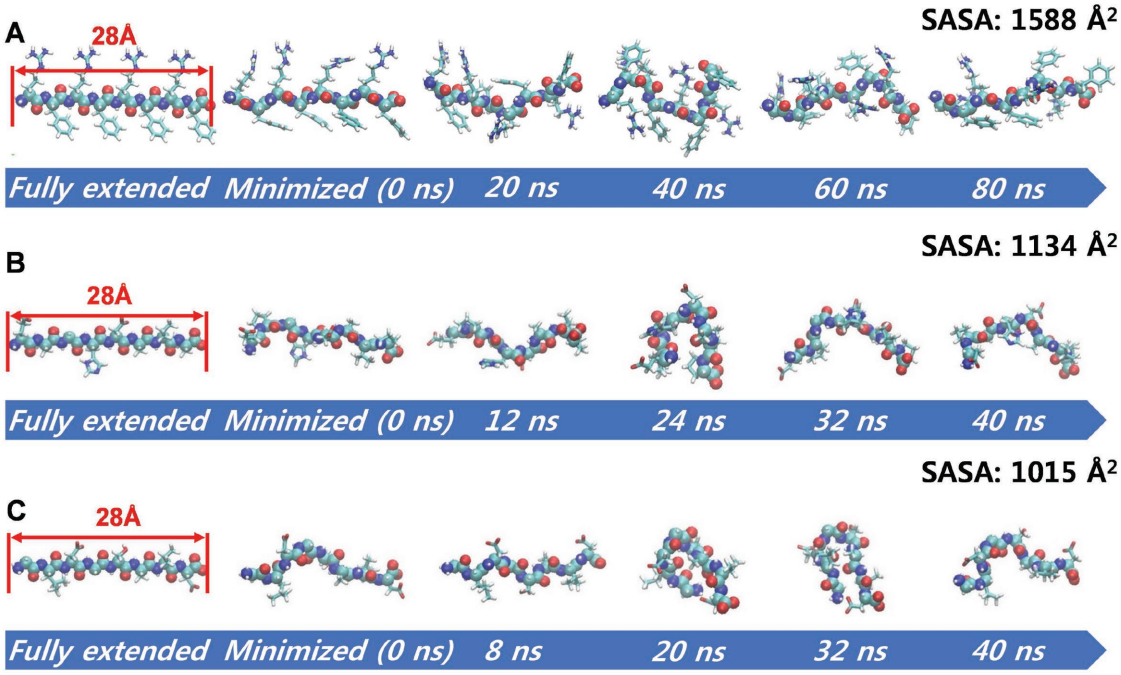

Figure 4. MD simulation results of octapeptides in water. Conformational changes in both backbone and side chains of: A) RF8, B) Copep, and C) random peptides. Average solvent-accessible surface area for 40 ns is calculated.

(13.17 and 3.6 Å) peptides. Therefore, this indicates that Copep and random peptides can exhibit more compact conformation than RF8. When the peptides are confined between GO sheets, the bulky side chain effect of RF8 could be intensified. As we confirmed in Figure 4A, the bulky side chains of RF8 are relatively difficult to fold into the galleries of the GO sheets under ambient pressure, while the flexible and small side chains of Copep and random peptides can be sufficiently folded between the GO sheets. The smaller channel sizes of GO-Copep and GO-random peptides were attributed to this weak side chain effect. This simulation result showed good agreement with the XRD experimental data. The unusually high compression of GO-RF8 at high pressure may be a result of its largest channel size, which was widened by the RF8 peptides. Because peptides are soft materials, they can be compressed into the galleries of GO laminates at high pressure, thus reducing the channels, particularly when the conformation is extended at low pressure and free space is available. This is the reason why GO-RF8 showed lower water permeation than GO-COOH at a relatively high pressure of 5 bar. Since Copep and random peptides are already compressed at ambient pressure, these peptides were not compressed anymore at high pressure of 5 bar, which is also reflected in the normal pressure response of the GO-Copep and Go-random membranes in Figure 2B. However, further studies are needed to investigate how the dynamic characteristics of peptides regulate flow through GO when pressure is changed.

When the permeate flux and separation performance of GO-based membranes were compared at 2 bar (Figure 2B), GO-RF8 showed superior water flux with the highest MB molecule rejection. At 2 bar, the permeated flux of the aqueous MB solution through GO-RF8 was 1075 LMH, and MB molecule rejection was 91%. The permeate flux of GO-COOH was only 227 LMH with an MB rejection of 75%. The flux of the GO-RF8 membrane was thus approximately fivefold that of GO-COOH. The permeate flux values of GO-Copep and GO-random were even lower. The high permeate flux of GO-RF8 may be related to its larger channel size. However, the channel size alone cannot fully explain the flux increase in GO–peptide membranes because GO-Copep and GO-random also have larger channels than GO-COOH but show lower permeation.

Considering GO-COOH, GO-Copep, and GO-random, peptide-functionalized GO showed lower flux and higher rejection rates for the MB molecules than GO-COOH, even with larger interplanar distances. This can be explained by considering the internal structure of the galleries of GO–peptide membranes. Although interplanar distances were widened by the peptide anchored to the GO channel surface, the galleries were not exclusively free space but were partially covered by the peptides. Therefore, despite the higher interplanar distances, the effective cross-sectional channel size of GO-Copep and GO-random for MB and water molecules may be smaller than that of GO-COOH. The Copep and random peptides anchored on the channel surface simultaneously widen the interplanar space and limit the permeation of all molecules, including water, leading to a lower flux and a higher rejection rate. This might be the reason why GO-GOOH showed a higher water flux than GO-Copep and GO-random at both 2 and 5 bar.

The rationale described above does not apply to GO-RF8 because GO-RF8 has the largest channel size, highest flux, and highest rejection. The performance of GO-RF8 suggests that RF8 peptides tethered to the GO surface have widened channels and exhibit restricted permeation of MB molecules, similar to Copep and random peptides (even more effectively), but they do not limit or facilitate the transport of water, unlike Copep and random peptides.

The better rejection of MB molecules by RF8 than the Copep and random peptides cannot be explained by a simple electrostatic mechanism. The net charges of Copep and random are negative, while RF8 peptides have positive charges. Because MB molecules are negatively charged, GO-Copep and GO-random membranes were expected to show better rejection properties than GO-RF8 membranes because of repulsion. It may be expected that negatively charged MB is attracted to the positive charge of RF8 peptides and becomes trapped, resulting in lower MB transport through the channel. However, trapped MB molecules would partially block the channel, significantly reducing the flux. In a previous report, trapped molecules reduced flux by half while simultaneously enhancing rejection rates.[34]

The better rejection of the GO-RF8 membranes may be a result of the better sieving mechanism. Normal sieving through pores occurs when the size of molecules being transported is smaller than the pore size. However, the interplanar spacing in GO–peptide membranes is not fully empty and is partially covered by peptides, as described above. The criteria for sieving in these membranes are not simply determined only by the channel size. Dynamic coverage of the channel with peptides is rather important. Although the interplanar distance of GO-RF8 is the largest, RF8 peptides have more bulky side chains than those of Copep and random peptides (Figure 4a). The side chains can effectively block the entrance of MB molecules. Therefore, the higher rejection rate of GO-RF8 membrane was attributed to the special sieving characteristics of RF8 peptides.

Notably, a superior permeate flux was observed for GO-RF8 membranes. The channel size of GO-RF8 is two-fold larger than that of GO-COOH, but the flux is approximately fivefold higher than that of GO-COOH. This suggests that water transport is facilitated in GO-RF8 membranes. In addition, while the partial coverage of the galleries between the GO layers by Copep and random peptides hinders the passage of both water and dye molecules, the bulky side chains of RF8 only restricts the passage of dye molecules while allowing or even facilitating the transport of water. There are two possible explanations for this superior water permeation with high rejection of dye molecules in GO-RF8 membranes. Because RF8 was designed to emulate the Ar/R water-selective filter of AQPs, the chemical nature of R and F amino acid residues may induce the rapid transport of water while rejecting other molecules, as in natural AQPs. In the Ar/R water-selective filter, the hydrophobic aromatic phenylalanine facilitates water transport while rejecting other polar ions. The positively charged arginine electrostatically repulses positive ions. The RF8 peptides tethered on the GO surface may function similarly by boosting water transport and simultaneously hindering MB molecule movement. However, we cannot exclude a second possibility that flux increased because of the enlarged channels by RF8. The Copep and random peptides disturb the passage of both water and MB molecules, likely because most of the space between GO layers is covered by hardly compressible, folded Copep and random peptides. However, the extended conformation of RF8 peptides widens the channel considerably and makes RF8 compressible, as demonstrated by the pressure response of GO-RF8. In this channel structure, there may be holes with a size appropriate for small molecule water to escape from the peptide net; however, large MB molecules (≈2 nm) are caught and thus filtered by the side chain net of RF8. If the latter explanation applies, however, the flux increase of GO-RF8 would be proportional to the channel size increase from GO-COOH, which is not the case as described above. Thus, facilitated water transport enabled by RF-8 peptides occurs.

In addition to facilitated water transport in GO-RF8, GO-COOH and GO-RF8 showed reversed changes in flux with increasing pressure. To investigate the differences in water transport between these membranes, we conducted water transport MD simulations for the GO-COOH and the GO-RF8 membranes. **Figure 5**A presents GO membrane models

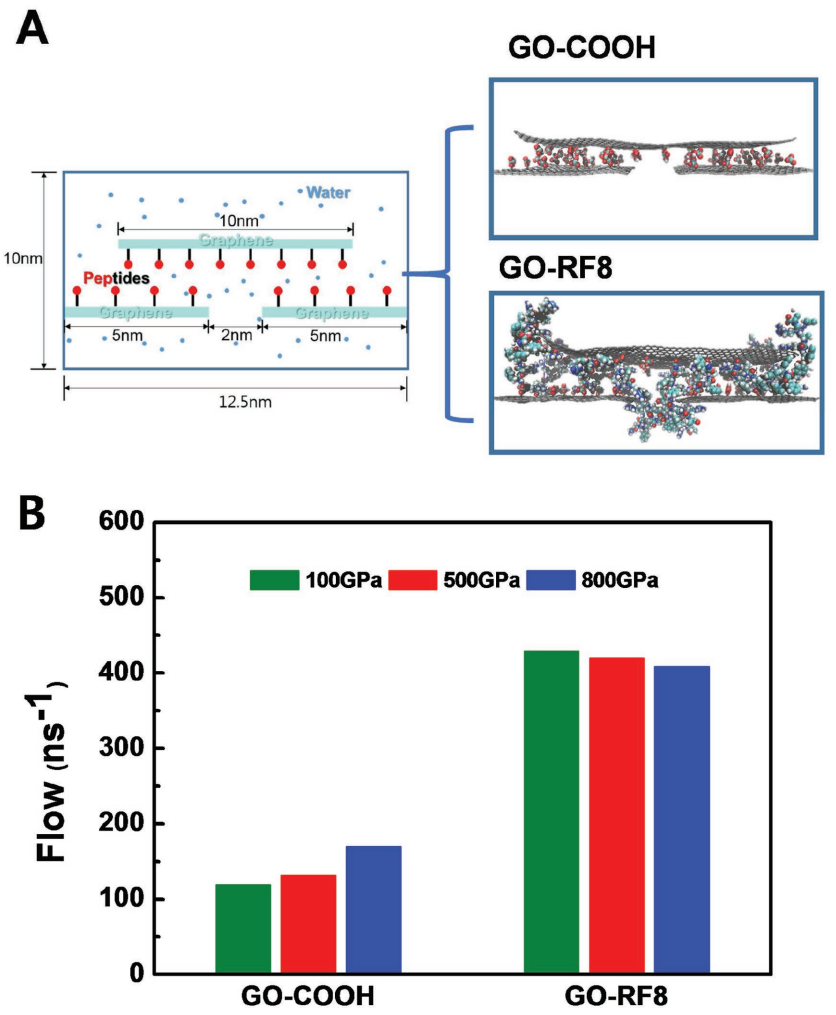

Figure 5. MD simulation results of GO-GOOH and GO-RF8. A) System configuration (left) and GO-COOH and GO-RF8 models (right). B) Water flow comparison.

(GO-COOH and GO-RF8) for water permeation simulation. As shown in Figure 5A, water molecules pass through GO membranes based on pressure differences. For GO-RF8, the distance between two GO layers was 1.624 nm, which is shorter than the backbone length of RF8 (≈2.7 nm). Thus, RF8 is somewhat folded and occupies significant space in the membrane. This occupation would affect the water transport through the membrane. Water molecules passing through the entire membrane were counted as flow in this simulation. As shown in Figure 5B, the water flow of GO-RF8 generally overrides the flow of GO-COOH. At low pressure, the water flow of GO-RF8 is more than 3.5-fold that of the GO-COOH. This implies that RF8 peptides in the GO membrane facilitate water transport, to some extent, chemically (Ar/R selective filter) and mechanically (larger channel size). However, the water flow increases far surpassed the channel size increase, clearly demonstrating the chemical support of the RF water-selective filter in facilitated water transport. Moreover, as the pressure difference increased, the water flow of GO-RF8 gradually decreased, while GO-COOH behaved in the opposite manner. This simulation result agrees well with the experimental data. Water transport in GO-RF8 may be impeded by densely packed RF8 peptides when GO membranes are compressed under higher pressure differences.

In conclusion, we evaluated the feasibility of artificially achieving the function of AQPs, a natural water-selective channel, by mimicking the Ar/R water-selective filter of AQP. The RF8 peptide motif designed was integrated with a GO platform by surface chemical modification. The resulting GO-RF8 membranes showed superior water permeation and good rejection properties of the dye molecules. Notably, the permeated flux was approximately fivefold that of GO-COOH with a higher rejection of dyes. Generally, the permeate flux and rejection are mutually exclusive properties that show opposite trends in most artificial membranes. Using specialized filter molecules on the surface emulating the function of AQPs, GO-RF8 achieved superior flux and high rejection, as in natural AQPs. The unique behavior of AQP-mimicking peptides was verified by computational analysis. MD simulation revealed the configuration of peptides and the behavior of water in 2D confined channels such as in GO–peptide membranes. Rather than transferring the whole AQP from natural cells, we successfully mimicked the core function of the AQP using simple short peptides. This study thus demonstrates the potential for reproducing the AQP function out of cell membranes based on a simple design. Using the pore platform with desirable dimensions, we hope to extend this toolkit for water purification applications.

Experimental Section

Fabrication of GO-Based Membranes: Graphene oxide was synthesized by a modified Hummers' method, as reported previously.[26] To increase the number of carboxylic groups of GO at the tethering points of peptides, we converted the ester, hydroxyl, and epoxide groups of GO to carboxyl groups by treating with $ClCH_2COONa$ and HCl. 5 g of $ClCH_2COONa$ and 5 g of NaOH were added to 100 mL of aqueous GO solution at a concentration of 1 mg mL^{-1}.[35] The mixture was sonicated in a bath for 2 h. The resulting solution was neutralized with 1 M HCl to form carboxylated GO (GO-COOH, hereafter). Rinsing and centrifugation were repeated to purify the product. Next, 100 mL of phosphate buffer (pH 7.4) was added to the final sediment to form a well-dispersed GO-COOH solution. Carbodiimide coupling chemistry was used to attach peptide motifs to GO-COOH.[24] Briefly, 20×10^{-3} M of 1-ethyl-3-(3-dimethlyaminopropyl)-carbodiimide (EDC) and 5×10^{-3} M of *N*-hydroxysuccinimide (NHS) were dissolved in 50 mL of phosphate buffer. The EDC/NHS solution was stirred with 50 mL of 1 mg mL^{-1} GO-COOH solution for 10 min, bath-sonicated for 1 h, and stirred for another 10 min. The final product was washed several times to discard excess EDC and NHS. The sediment was dissolved in 50 mL of deionized water. The 1×10^{-3} M peptide was dissolved in 50 mL of deionized water, and 0.01 M aqueous NaOH was added to the peptide solution to obtain a final pH of 8. The peptide solution was mixed with EDC-NHS-activated GO-COOH and stirred overnight. Excess peptides and ions were removed by washing three times with deionized water. The final solid product of the GO–peptide conjugate was dispersed in deionized water and diluted to 0.05 mg mL^{-1}. The solution pH was controlled by adding 0.01 M NaOH or 0.01 M HCl and tip-sonicated for 1 h to form a well-dispersed colloidal solution. The GO–peptide solution was vacuum filtered through a PC or MCE membrane with a pore size of 0.2 µm. The typical loading amount was 0.1 mg cm^{-2}.

Characterization: The thickness and surface morphology of GO-based membranes were examined by scanning electron microscopy (SEM, Hitachi S-4800, Tokyo, Japan). Chemical analysis by X-ray photoelectron spectroscopy was performed on a Thermo VG K-alpha (Thermo Scientific, Waltham, MA, USA). The GO-based membranes were also characterized by X-ray diffraction (Rigaku SmartLab, Tokyo, Japan). The zeta potential of each GO-based solution was recorded on an Otsuka Electronics ELSZ-1000 (Tokyo, Japan). The concentration of transported methyl blue molecules through GO-based membranes was determined by UV–vis (JASCO, V-650, Oklahoma City, OK, USA) absorption measurements.

Permeation Test: The permeation test was conducted using a stirred cell (STERLITECH HP4750 Stirred cell, Kent, WA, USA) with a membrane area of 3.9 cm^2. The GO-based membrane supported on PC or MCE was installed at the bottom of the stirred cell. Pressure was applied using nitrogen gas from 1.5 to 5 bar. The permeate flux of pure water was estimated by weighing the permeated solution through the membrane every 5 min. Methyl blue molecule rejection was measured similarly. The membrane was exposed to 20×10^{-6} M methyl blue solution, and pressure was applied. The mass of the permeated solution and the concentration of methyl blue molecule were measured every 5 min. The concentration of methyl blue was evaluated by UV–vis spectroscopy.

Molecular Dynamics Simulation: All peptide models (RF8, Copep, and random) and GO models (GO-COOH and GO-RF8) were constructed by Avogadro.[36] Topology data for each peptide model were obtained from an automatic OPLS-AA topology generator web program, TPPMKTOP, developed by the ERG research group.[37,38] Simulations were conducted using NAMD v2.10[39] for the peptide models and GROMACS-5.1.2[40] for the GO models.

For each peptide model, energy minimization was conducted for 50 ps, and an equilibration simulation was then performed for 80 ns in the simulation box (initially $5 \times 5 \times 5$ nm^3) with a periodic boundary condition and isothermal–isobaric (NPT) ensemble. The time step of the simulations was 2 fs. The temperature was kept in 300 K by Langevin dynamics with damping coefficient as 1 ps^{-1}. Pressure was kept in 1.01325 bar (1 atm) by the Langevin piston Nosé–Hoover method.[41] The TIP3P model[42] was applied for water molecules. A full electrostatic calculation was performed at every step by the smooth particle mesh Ewald method[43] with an interpolation order of 6. Each GO model system consists of one large upper GO layer (10×4 nm^2) and two small lower GO layers (5×4 nm^2) located in the simulation box ($12.5 \times 4.5 \times 10$ nm^3) with a periodic boundary condition. Simulations were performed for 50 ns. In Figure S4 (Supporting Information), 24 COOH molecules (3×8, carboxyl group) were attached to the graphene with a uniform space of 1.2 nm in the large GO-COOH layer, while 12 COOH molecules were attached to each small GO-COOH layer with the same spacing. Next, 8 (4) COOH

molecules in the large (small) GO-COOH model were replaced with RF8 peptides to construct the large (small) GO-RF8 model. To simulate the experimental conditions, the gap distance between the upper and lower GO layers was set to 0.87 and 1.62 nm for GO-COOH and GO-RF8, respectively, and each carbon atom in the GO layer was anchored at its initial position with a linear spring of which the stiffness value was 1000 kJ mol^{-1} nm^{-2}, to sustain the GO layers in space. Hydrostatic pressure differences across the GO membrane were induced, as described by Zhu et al.,[44] which has been used in many previous membrane simulations.[45–52] In this method, a constant force, f, was applied to each water molecule along the z-direction to produce a hydrostatic pressure across the membrane, as shown in Figure S5 (Supporting Information). If P_1 and P_2 denote pressure, respectively, at the lower and upper parts of the membrane, $-P_1A + P_2A + nf = 0$, then the pressure difference is given by $\Delta P = P_1 - P_2 = nf/A$, where ΔP is the pressure difference across the membrane, n is the number of water molecules in the simulation box, and A is the cross-sectional area of the system. The time step for this simulation was 2 fs. Simulations were performed under the canonical (NVT) ensemble. Temperature was kept at 300 K using the velocity rescaling thermostat.[53] The expanded simple point charge (SPC/E) water model[54] was applied for these simulations. The long-range electrostatics were calculated by the smooth particle mesh Ewald method[43] with an interpolation order of 4. For the simulation speed, LINear Constraint Solver[55] was used. System visualization, SASA calculation, and end-to-end distance measurement were all performed by visual molecular dynamics (VMD).[56]

Supporting Information

Supporting Information is available from the Wiley Online Library or from the author.

Acknowledgements

C.S.L. and M.-K.C. contributed equally to this work. This research was supported by the Pioneer Research Center Program supported by the National Research Foundation of Korea (NRF) and Korean Ministry of Science and ICT (MSIT) (Grant Nos. NRF-2012-0009577 and NRF-2012-0009579).

Conflict of Interest

The authors declare no conflict of interest.

Keywords

biomimetic, graphene oxide, membranes, recognition, selectivity

Received: October 12, 2017
Revised: November 28, 2017
Published online:

[1] D. Seckler, R. Barker, U. Amarasinghe, *Int. J. Water Resour. Dev.* **1999**, *15*, 29.
[2] H. W. Liang, X. Cao, W. J. Zhang, H. T. Lin, F. Zhou, L. F. Chen, S. H. Yu, *Adv. Funct. Mater.* **2011**, *21*, 3851.
[3] J. Mulder, *Basic Principles of Membrane Technology*, Kluwer Academic Publisher, Dordrecht, The Netherlands **1996**.
[4] J. Zhao, X. Zhao, Z. Jiang, Z. Li, X. Fan, J. Zhu, H. Wu, Y. Su, D. Yang, F. Pan, *Prog. Polym. Sci.* **2014**, *39*, 1668.
[5] C. Y. Tang, Y. Zhao, R. Wang, C. Hélix-Nielsen, A. G. Fane, *Desalination* **2013**, *308*, 34.
[6] L. F. Greenlee, D. F. Lawler, B. D. Freeman, B. Marrot, P. Moulin, *Water Res.* **2009**, *43*, 2317.
[7] M. Elimelech, W. A. Phillip, *Science* **2011**, *333*, 712.
[8] M. M. Pendergast, E. M. V. Hoek, *Energy Environ. Sci.* **2011**, *4*, 1946.
[9] K. P. Lee, T. C. Arnot, D. Mattia, *J. Membr. Sci.* **2011**, *370*, 1.
[10] S. S. Shenvi, A. M. Isloor, A. Ismail, *Desalination* **2015**, *368*, 10.
[11] H. Ma, C. Burger, B. S. Hsiao, B. Chu, *ACS Macro Lett.* **2012**, *1*, 723.
[12] S. Qi, R. Wang, G. K. M. Chaitra, J. Torres, X. Hu, A. G. Fane, *J. Membr. Sci.* **2016**, *508*, 94.
[13] Y. Zhao, C. Qiu, X. Li, A. Vararattanavech, W. Shen, J. Torres, C. Helix-Nielsen, R. Wang, X. Hu, A. G. Fane, *J. Membr. Sci.* **2012**, *423*, 422.
[14] Y. Kaufman, A. Berman, V. Freger, *Langmuir* **2010**, *26*, 7388.
[15] M. Kumar, M. Grzelakowski, J. Zilles, M. Clark, W. Meier, *Proc. Natl. Acad. Sci. USA* **2007**, *104*, 20719.
[16] K. Murata, K. Mitsuoka, T. Hirai, T. Walz, P. Agre, J. B. Heymann, A. Engel, Y. Fujiyoshi, *Nature* **2000**, *407*, 599.
[17] P. Agre, S. Sasaki, M. J. Chrispeels, *Am. J. Physiol.* **1993**, *265*, F461.
[18] A. S. Verkman, A. K. Mitra, *Am. J. Physiol. - Renal Physiol.* **2000**, *278*, F13.
[19] J. S. Hub, B. L. De Groot, *Proc. Natl. Acad. Sci. USA* **2008**, *105*, 1198.
[20] B. L. de Groot, H. Grubmüller, *Science* **2001**, *294*, 2353.
[21] Y. X. Shen, P. O. Saboe, I. T. Sines, M. Erbakan, M. Kumar, *J. Membr. Sci.* **2014**, *454*, 359.
[22] P. Sun, M. Zhu, K. Wang, M. Zhong, J. Wei, D. Wu, Z. Xu, H. Zhu, *ACS Nano* **2013**, *7*, 428.
[23] K. P. Loh, Q. Bao, G. Eda, M. Chhowalla, *Nat. Chem.* **2010**, *2*, 1015.
[24] H. Wang, Q. Zhang, X. Chu, T. Chen, J. Ge, R. Yu, *Angew. Chem., Int. Ed.* **2011**, *50*, 7065.
[25] L. Zhang, J. Xia, Q. Zhao, L. Liu, Z. Zhang, *Small* **2010**, *6*, 537.
[26] M. Hu, B. Mi, *Environ. Sci. Technol.* **2013**, *47*, 3715.
[27] L. Qiu, X. Zhang, W. Yang, Y. Wang, G. P. Simon, D. Li, *Chem. Commun.* **2011**, *47*, 5810.
[28] S. Kim, J. Nham, Y. S. Jeong, C. S. Lee, S. H. Ha, H. B. Park, Y. J. Lee, *Chem. Mater.* **2015**, *27*, 1255.
[29] G. Eda, G. Fanchini, M. Chhowalla, *Nat. Nanotechnol.* **2008**, *3*, 270.
[30] D. H. Everett, *Basic Principles of Colloid Science*, Royal Society of Chemistry, London **1988**.
[31] Y. Huang, C.-Y. Chiang, S. K. Lee, Y. Gao, E. L. Hu, J. D. Yoreo, A. M. Belcher, *Nano Lett.* **2005**, *5*, 1429.
[32] D. L. Gin, R. D. Noble, *Science* **2011**, *332*, 674.
[33] R. Joshi, P. Carbone, F.-C. Wang, V. G. Kravets, Y. Su, I. V. Grigorieva, H. Wu, A. K. Geim, R. R. Nair, *Science* **2014**, *343*, 752.
[34] H. Huang, Z. Song, N. Wei, L. Shi, Y. Mao, Y. Ying, L. Sun, Z. Xu, X. Peng, *Nat. Commun.* **2013**, *4*, 2979.
[35] W. S. Hummers Jr., R. E. Offeman, *J. Am. Chem. Soc.* **1958**, *80*, 1339.
[36] M. D. Hanwell, D. E. Curtis, D. C. Lonie, T. Vandermeersch, E. Zurek, G. R. Hutchison, *J. Cheminform.* **2012**, *4*, 17.
[37] W. L. Jorgensen, D. S. Maxwell, J. Tirado-Rives, *J. Am. Chem. Soc.* **1996**, *118*, 11225.
[38] A. Nesterenko, TPPMKTOP, v. 0.6.2, http://erg.biophys.msu.ru/erg/tpp (accessed: May 2015).
[39] J. C. Phillips, R. Braun, W. Wang, J. Gumbart, E. Tajkhorshid, E. Villa, C. Chipot, R. D. Skeel, L. Kale, K. Schulten, *J. Comput. Chem.* **2005**, *26*, 1781.
[40] M. J. Abraham, T. Murtola, R. Schulz, S. Páll, J. C. Smith, B. Hess, E. Lindahl, *SoftwareX* **2015**, *1*, 19.
[41] G. J. Martyna, D. J. Tobias, M. L. Klein, *J. Chem. Phys.* **1994**, *101*, 4177.
[42] W. L. Jorgensen, J. Chandrasekhar, J. D. Madura, R. W. Impey, M. L. Klein, *J. Chem. Phys.* **1983**, *79*, 926.

[43] U. Essmann, L. Perera, M. L. Berkowitz, T. Darden, H. Lee, L. G. Pedersen, *J. Chem. Phys.* **1995**, *103*, 8577.
[44] F. Zhu, E. Tajkhorshid, K. Schulten, *Biophys. J.* **2002**, *83*, 154.
[45] J. Azamat, A. Khataee, S. W. Joo, *Chem. Eng. Sci.* **2015**, *127*, 285.
[46] J. Kou, X. Zhou, H. Lu, F. Wu, J. Fan, *Nanoscale* **2014**, *6*, 1865.
[47] J. Su, K. Yang, H. Guo, *Rsc. Adv.* **2014**, *4*, 40193.
[48] B. Liu, R. Wu, J. A. Baimova, H. Wu, A. W.-K. Law, S. V. Dmitriev, K. Zhou, *Phys. Chem. Chem. Phys.* **2016**, *18*, 1886.
[49] D. Yang, Q. Liu, H. Li, C. Gao, *J. Membr. Sci.* **2013**, *444*, 327.
[50] Q. Chen, X. Kong, J. Li, D. Lu, Z. Liu, *Phys. Chem. Chem. Phys.* **2014**, *16*, 18941.
[51] M. Heiranian, A. B. Farimani, N. R. Aluru, *Nat. Commun.* **2015**, *6*, 8616.
[52] M. Ding, A. Szymczyk, A. Ghoufi, *Desalination* **2015**, *368*, 76.
[53] G. Bussi, D. Donadio, M. Parrinello, *J. Chem. Phys.* **2007**, *126*, 014101.
[54] H. Berendsen, J. Grigera, T. Straatsma, *J. Chem. Phys.* **1987**, *91*, 6269.
[55] B. Hess, H. Bekker, H. J. Berendsen, J. G. Fraaije, *J. Comput. Chem.* **1997**, *18*, 1463.
[56] W. Humphrey, A. Dalke, K. Schulten, *J. Mol. Graphics* **1996**, *14*, 33.